Modeling and observations of atmosphere-ionosphere response to earthquakes

P.A. Inchin[1], M.D. Zettergren[1], J.B.Snively[1], A.Komjathy[2], O.Verkhoglyadova[2]

(1) Embry-Riddle Aeronautical University, Daytona Beach, FL, USA
(2) Jet Propulsion Laboratory, California Institute of Technology, Pasadena, CA, USA
E-mail: inchinp@my.erau.edu

Context

Natural hazards serve as a source of disturbances to the solid (earthquakes, landslides), liquid (tsunamis) or gaseous (tornados, hurricanes, volcanic eruptions) envelopes of the Earth. As they couple with the atmosphere, these disturbances can drive acoustic and gravity waves (AGWs) that propagate to the upper atmosphere. Due to the conservation of energy, the decrease of density in the atmosphere with altitude results in exponential growth of these waves, triggering coseismic ionospheric disturbances (CID) in the overlying ionosphere which can be observed using in-situ or remote sensing instruments.

Earthquakes serve as a source of AGWs from intense near-field vertical displacements and from surface response to Rayleigh waves (RW) and body waves that propagate to far distances (although for the latter the atmospheric response is very weak). Inland large thrust earthquakes happen less frequently than oceanic ones. However, in the presence of appropriate seismic data, they allow studying the dynamic processes near the epicentral region and enable simulations of atmosphere-ionosphere response with high accuracy.

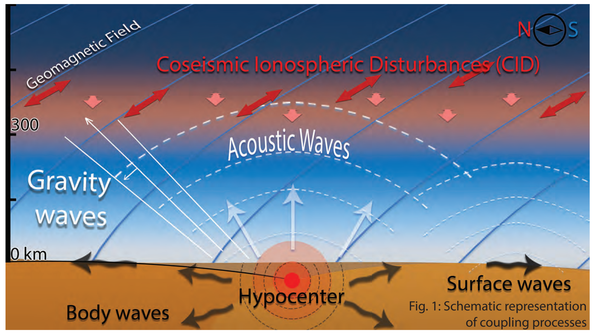

Fig. 1: Schematic representation of coupling processes

Study case

The Nepal 2015 Mw7.8 earthquake, also known as Gorkha earthquake, occured on 25th April 2015, was one of the most devastating earthquakes in the last century at Main Himalayan Thrust [Bilham et al., Sci, 2001], with around 4000 landslides and more than 3000 aftershocks within 45 days after the event [Kargel et al., Sci, 2016; Adhikari et al., GJI, 2015]. Large vertical displacements, with a trough-to-peak amplitude of ~1.6 m in the epicentral area [Lindsey et al., 2015], triggered atmospheric AGWs with amplitudes sufficient for their detection using GNSS TEC measurements in the near and far-field regions. Main information about the earthquake is presented in Table 1.

Table 1. Nepal Gorkha earthquake

Origin time	25.04.2015 11:56:25 NST (06:11:25 UTC)
Magnitude	7.8Mw Megathrust
Location	28.23°N / 84.73°E
Strike/Dip/Slip	290°/7°/101°
Depth	~12-25 km, Main Himalayan Thrust

Modeling approach

To simulate realistic responses, we combine three numerical models spanning from the Earth's surface, to its atmosphere, and ionosphere. The surface dynamics, calculated based on SPECFEM3D-Globe (bottom surface of the cube on figure) seismic waves propagation model [Komatitsch and Tromp, JGI, 2002a] is incorporated into the 3D neutral atmosphere model MAGIC (domain shown as a cube) to simulate atmospheric dynamics, acoustic and gravity wave generation, propagation, and dissipation [Snively, JGR, 2013]. Subsequently we do a slice along longitude of interest from 3D MAGIC simulation and use it as an input to 2D GEMINI model (tilted dipole) which encapsulates the ionospheric response to neutral forcing through neutral drag, dynamo currents, and modifications to thermospheric densities [Zettergren and Semeter, JGR, 2012]. The coupled MAGIC-GEMINI model enables realistic simulation of atmosphere-ionosphere responses to ground-based and tropospheric perturbations [Zettergren and Snively, JGR, 2015; Zettergren et al., JGR, 2017]. Simulations results are supported by GNSS TEC measurements and seismometers data. Results show the complexity of lithosphere-atmosphere-ionosphere coupling and motivate further investigations of this interconnection and resulting observable signatures.

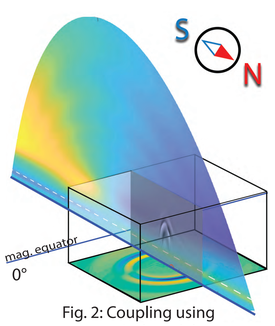

Fig. 2: Coupling using numerical models

Earthquake description

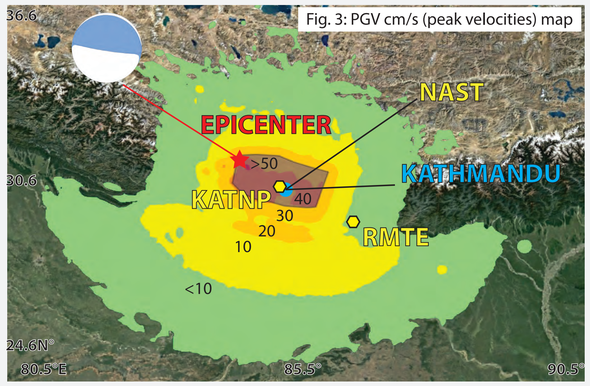

Based on USGS solution (Table 1), the focal mechanism of the earthquake is of thrust fault type with low dip angle (6-7°). Finite-source rupture modeling results show that rupture nucleated near the hypocenter and propagated along downdip direction to South-East for 140-160km (50-60 cross-strike extent) with velocity of 2.5-3.2 km/s [Zhang et al., 2015; Fan et al., 2015; Yue et al., 2016; Wei et al., 2017]. The earthquake ruptured only a deep part of seismogenic zone [Kobayashi et al., 2015; Wang and Fialko, 2016]. The vertical velocities, found from strong motion accelerometers data and GNSS highrate measurements at near-epicentral regions, were up to 65cm/s (Fig. 3); this is an important indicator of the possibility of AGWs exitation [Takai et al., 2016].

Observations

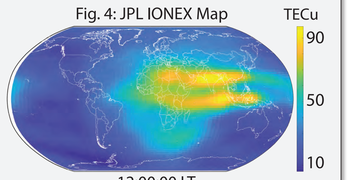

Fig. 4: JPL IONEX Map

The earthquake happened during magnetic quite daytime conditions, with Ap index: ~2 and F10.7 index of 127.4. Absolute vTEC was ~75TECu near the epicentral region due to the effect of equatorial anomaly (Fig. 4). The maximum vertical TEC (vTEC) at the North crest of ~17° was up to 90 TECu. We used 0.2/30 sec GNSS data to calculate vTEC absolute values (Fig. 6). Ionospheric pierce point (IPP) positions for all stations on Fig. 7 were at the latitude of epicenter or to the North of it. Coseismic ionospheric disturbances (CID) were observed mostly to the East from the epicenter, whereas to the West no observable perturbation were registered (GRHI, DNSG, LCK3 stations). Elevation angles for all IPP positions shown were >50° (expect LCK4 with ~30°).

CID near the epicentral region were registered up to 1.6ptp TECu with periods of ~3.3-8 min (Fig. 6) 9-10 min after the earthquake. Data for stations BRN2, LCK3 were filtered with 10 min Gaussian filter (Fig. 5).

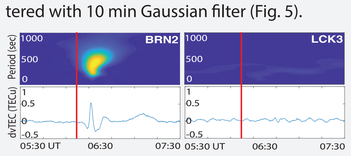

Fig. 5: Data for station to East (left) and West (right) from epicenter

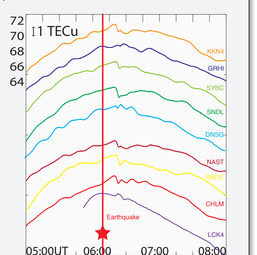

Fig. 6: Absolute vTEC

We found that the initial phase of CID to the North from epicenter latitude was a rarefaction leading to reduced TEC, whereas to the South, initial phase of CID was a compression (e.g. stations BRN2 and KKN4 respectively on Fig. 5).

Fig. 7: IPP TEC map

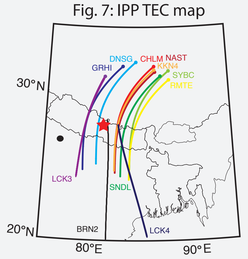

Catherine et al. [2016] and Chen et. al. [2017] reported common CIDs of ~1.5TECu ptp amplitude and velocities of 800-1200 m/s at near-epicentral regions and ~2.2-2.7 km/s at larger distances that were attributed to RW due to high phase velocity. Tulasi et al. [2017] mentioned that the velocity of RW CID is not consistent with velocities of RW propagation at observable in CID periods from seismic data.

Surface response simulation results

We used finite fault solution provided by USGS, which consists of 196 point sources with appropriate positions, moment tensors, half-durations and timing (Fig. 9). Synthetic seismograms were calculated for every point on a grid of 2000x760 km with spatial step of 2 km using SPECFEM3D-Globe. Simulation is accurate for wave periods up to 14 sec. 3D Earth model (S362ANI) with appropriate 1D Crust model was used. To eliminate boundary reflection effects, a global simulation was performed. Results show that the simulation preserved the direction of rupture propagation and predominant surface wave directivity to South-East (Fig. 8a-d), specially on periods of 50-80 sec. Simulation showed slightly lower vertical velocities at near-field region (Fig. 8e) than those registered using GNSS stations, probably because USGS did not use near-field data.

Fig. 8: Simulations results for surface vertical velocities

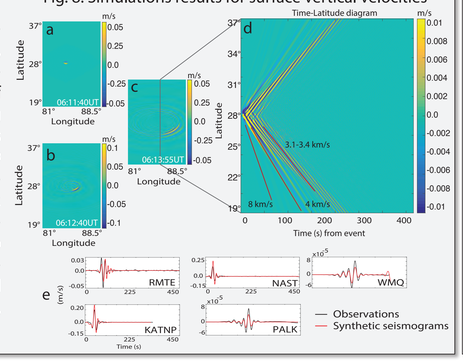

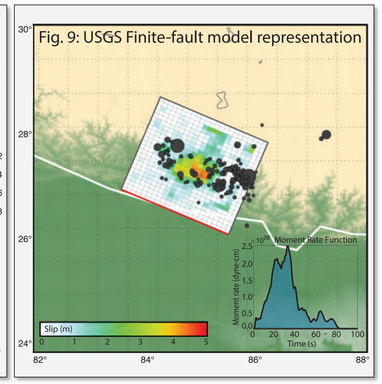

Atmosphere-ionosphere near-field response simulation results

According to simulations, the earliest observable vTEC perturbations are found ~9 min after the nucleation of the rupture. South-North assymetry in electron density can be seen (Fig. 10a-d). Near-field CID of ~1.8 ptp and 3.3 min and 0.98 km/s velocity, as well 0.3 ptp 8 min period and 230 m/s velocity are found from simulations (Fig. 11a-d). These obsevations are consistent with observations. The periods of CID are ~3.3min and 8-9min. Such parameters of near-field CID are common and supported by observations.

Fig. 10: Plasma velocity along magnetic field lines

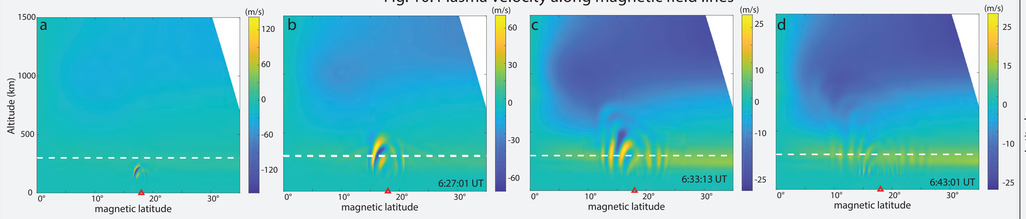

Fig. 11: Time-Latitude vTEC diagram

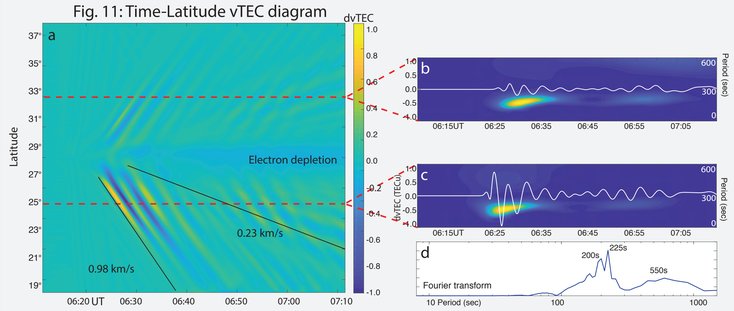

Simulation shows that coseismic crustal uplift near epicenter led to the initial compression phase of acoustic waves to East from strike direction, whereas subsidence generated acoustic waves with initial rarefaction mostly to North (Fig. 12). Rupture propagation to SSE from hypocenter also affected exitation of AGW (Fig. 13). Source of AGWs shifted for ~50 km to SSE; this is in accordance of earthquake's maximum energy release during ~20 seconds with rupture velocity ~3 km/s.

Fig. 12: z=250 km vertical fluid velocities (m/s)

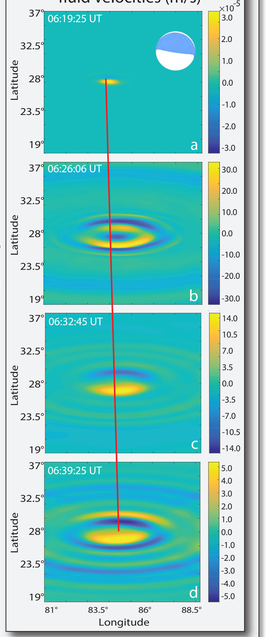

Fig. 13: Surface vertical (left) and z=250km fluid vertical velocities (right)

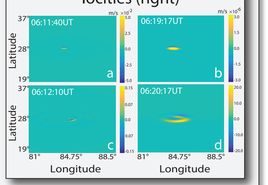

This simulation supports previous observational studies [Astafyeva and Heki, JGR, 2009]. Also, on Fig. 13 the propagation of CID wavefront to South-East from epicenter is shown what is consistent with GNSS TEC data observations.

Atmosphere-ionosphere response to Rayleigh waves

GNSS observations reports show in common that fast CID propagated with velocity of 2.2-2.7 km/s and was detected only to the South and East. Our simulation shows that directivity for long period Rayleigh waves plays role with only slightly higher amplitudes to South-East (Fig. 14). This is because most of the long period waves earthquake energy release was comparatively constained in time and space. The velocity of RW CID is ~4 km/s and consistent with the surface velocity of RW. Results show low amplitudes of vertical fluid velocities - 15 m/s ptp. The elevation angle of driven acoustic wave wavefront is ~6° at surface and ~14° (Fig.15a-b) at ionospheric heights which makes them detectable mostly for IPP elevation angle <30° with surface. The underestimation of the velocities in real data might be connected with inappropriate choice of altitude of ionospheric shell with which the perturbations are linked and increased IPP velocities for low elevation angles [Savastano, Tesi di Dottorato, 2018]. For low elevation angles the IPP velocity magnitude can be up to 0.5 km/s. Longer period of observed RW CID (~434s [Reddy et al., JGR, 2015]) than those found in simulation (~220s) corroborates this idea (due to Doppler shift effect). The complexity of Indian plate and high Himalaya region might also play imporant role. Lack of data attributes to difficulty of the analysis of RW for this earthquake.

Fig. 14: Time-latitude diagram of z=350km vertical fluid velocities

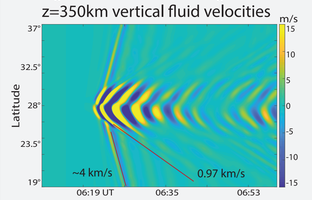

Fig. 15: Latitude-altitude slice for 87°E longitude of vertical fluid velocities

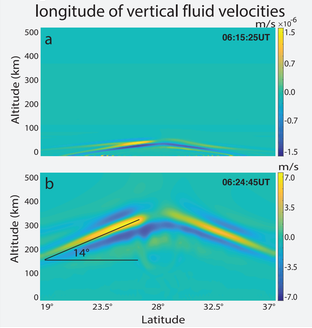

Discussion and future work

- Atmosphere-ionosphere response to ground-level displacements caused by Nepal 2015 Gorkha earthquake was simulated;
- Near-field vTEC perturbations are consistent with observations in frequencies, velocities and amplitudes;
- Strike directivity of earthquake, as well rupture propagation affect the exitation of near-field CID;
- We showed that the velocity of RW CID is constained by the velocity of RW on the surface (~4 km/s) that supports previous studies [e.g. Rolland et al., JGR, 2011]. Deep analysis of RW CID is needed with 3D ionospheric model;
- Detailed earthquake rupture modeling for which inversion was performed based on near-epicentral data will be used for further simulations [e.g. Yue et al., 2016].

Acknowledgements

Seismometers data were provided by IRIS services. The facilities of IRIS Data Services and the IRIS DMC were used for access to waveforms, related metadata, and/or derived products used in this study. GNSS data were obtained using UNAVCO Facility with support from the NSF and NASA under NSF Cooperative Agreement No. EAR-0735156. KATNP accelerometer data were obtained through www.strongmotioncenter.org. cGNSS data processed using PPP Kinematic service provided by Natural Resources Canada. Finite fault model was provided by USGS service supported by NEIC of USGS. Research was supported by NASA grant NNX14AQ39G to ERAU and NNH15ZDA001N-ESI via subcontract from JPL. Models used in this study were developed under support from NSF CAREER grants AGS-1255181 and AGS-1151746.